



Polypyrrole/bacterial cellulose nanofiber composites for hexavalent chromium removal

Yatao Shao · Zhihong Fan · Mingfeng Zhong · Wei Xu · Chang He · Zhijie Zhang

Received: 4 August 2020 / Accepted: 12 December 2020 / Published online: 15 January 2021
© The Author(s), under exclusive licence to Springer Nature B.V. part of Springer Nature 2021

Abstract Polypyrrole/bacterial cellulose (PPy/BC) composites with nanofiber structure were prepared by a facile in situ oxidative polymerization for the efficient removal of hexavalent chromium (Cr(VI)) from aqueous solution. The characteristics of the adsorbent were analysed by SEM, TEM, BET, EDX, FT-IR, and XPS and PPy found to be evenly wrapped on cellulose surfaces to form a core-shell structure and the specific surface area calculated at $95.9 \text{ m}^2 \text{ g}^{-1}$. Benefiting from high surface area, PPy/BC efficiently removed Cr(VI) and possessed a maximum adsorption capacity of 555.6 mg g^{-1} at 298 K and pH 2. Adsorption data was determined to conform to the Langmuir isotherm model and pseudo-second-order model. Cr(VI) adsorption on PPy/BC was involved in ion exchange and electrostatic attractions. Meanwhile, a portion of Cr(VI) was reduced to trivalent chromium (Cr(III)) by pyrrolic nitrogen and then retained on

PPy/BC surfaces by chelation. In addition, PPy/BC maintained 70.5% of its initial adsorption capacity after five adsorption and desorption cycles. This study demonstrated that PPy/BC can be a cost-effective, reusable, and highly efficient adsorbent for Cr(VI) removal.

Keywords Polypyrrole · Bacterial cellulose · Nanofiber · Adsorption · Cr(vi)

Introduction

Due to rapid industrialization and population pressure, large amounts of wastewater containing heavy metal ions have entered into the ecological water environment. As one of the most toxic contaminants in water, chromium(VI) (Cr(VI)) is carcinogenic and teratogenic for human beings (Zhang et al. 2010; Huang et al. 2019). In aqueous solution, chromium ions are usually in two valence states, Cr(VI) and Cr(III), but Cr(VI) is much more toxic and mobile in the environment than Cr(III) (Guan et al. 2019). The World Health Organization (WHO) recommends that the concentration of total Cr in industrial wastewater should be $< 0.1 \text{ mg/L}$ and the maximum allowable total chromium concentration in drinking water should be $< 0.05 \text{ mg/L}$ (H. Demiral et al. 2008). Therefore, exploring ways to effectively remove Cr(VI) from water has become an urgent issue.

Supplementary Information The online version of this article (<https://doi.org/10.1007/s10570-020-03660-2>) contains supplementary material, which is available to authorized users.

Y. Shao · M. Zhong · W. Xu · C. He · Z. Zhang (✉)
School of Materials Science and Engineering, South China University of Technology, Guangzhou 510640, China
e-mail: imzhang@scut.edu.cn

Z. Fan
Key Laboratory of Harbor and Marine Structure Durability Technology Ministry of Communications, Guangzhou 510230, China

Various methods, including precipitation (Gheju and Balcu 2011), electrochemical treatment (Jin et al. 2016), photocatalytic reduction (Xu et al. 2019), and adsorption (Zhang et al. 2019), have been applied to reduce Cr(VI) presence in water. In general, an adsorption method is more promising because it can involve many inexpensive, green, and renewable materials as adsorbents (Jin et al. 2017).

In the past few years, conducting polymers such as polypyrrole (PPy), polythiophene (PTH) and polyaniline (PANi) have attracted much attention to removing heavy metals from water due to their advantages of high adsorption capacity and easy synthesis (Molaei et al. 2017). PPy is very suitable for the removal of Cr(VI) from water, which is attributed to the inherent properties like high chemical stability and good ion exchange performance (Mahmud et al. 2016). However, in the polymerization process, pyrrole easily agglomerates into particles, with a specific surface area of PPy usually of only $12.21 \text{ m}^2 \cdot \text{g}^{-1}$ and the adsorption capacity of Cr(VI) at only $21.87 \text{ mg} \cdot \text{g}^{-1}$ (Roy et al. 2012). Therefore, scientists have been trying to use templates to expand PPy specific surface area, thus improving its adsorption performance. Fang et al. have synthesized graphene/SiO₂@PPy nanocomposites with a specific surface area of $37.6 \text{ m}^2/\text{g}$ and these adsorbents exhibit good adsorption performance (429.2 mg g^{-1} ; Fang et al. 2018). Ko et al. have prepared PPy/carbon black composite particles with a specific surface area of $64.47 \text{ m}^2 \cdot \text{g}^{-1}$ and adsorption capacity that reaches 174.8 mg g^{-1} (Ko et al. 2018). Although the PPy specific surface area is improved to a certain extent when spherical or sheet materials are used as templates, agglomeration is still difficult to avoid, and difficult to separate from solution after adsorption. This not only reduces the adsorption performance of PPy particles, but also limits its application in the removal of Cr(VI). To further improve the accessibility of adsorption sites, nanofibers have been used as templates; for instance, PPy-wrapped oxidized MWCNTs nanocomposites and bamboo-like PPy nanotubes exhibit adsorption capacities at 294.1 and 482.6 mg g^{-1} , respectively (Bhaumik et al. 2016; Li et al. 2012). However, the cost of the above-mentioned fiber templates has been relatively high and local pyrrole agglomeration still difficult to avoid. So, it is essential to develop high-efficiency and low-cost PPy adsorbents.

Bacterial cellulose (BC), which has a 3D nanofiber-network structure, is one of the most abundant, renewable, natural celluloses (Wu et al. 2015). It has higher purity, crystallinity, Young's modulus value and aspect ratio. After compounding with other materials, it can increase the strength and stability of the composite material and is a good chemical reaction template (Wang et al. 2019). BC is rich in hydroxyl groups and can form hydrogen bonds with –NH– groups in pyrroles, which can serve to limit irregular agglomeration of PPy and might improve its adsorption properties. To our knowledge, there has been no study to date regarding the removal of Cr(VI) using PPy/BC nanofiber composites.

In this study, PPy/BC nanofiber composites were prepared by an in situ oxidation polymerization and its properties examined using various characterization methods. The adsorption performance and mechanism of PPy/BC for Cr(VI) were then analysed and discussed.

Experimental section

Materials

The foodstuff Nata de coco was purchased from Yeshen Food Co., Ltd. (Shanghai, China). Pyrrole monomer (Py, 99%), potassium dichromate (K₂Cr₂O₇), 1,5-diphenylcarbazine, ammonium persulfate (APS), and anhydrous ferric chloride (FeCl₃) were purchased from Aladdin Reagent Co., Ltd. (Shanghai, China). All other reagents were used as received, unless stated otherwise.

Preparation of PPy/BC

According to the method reported by Sai et al. (2015), BC hydrogel was prepared using Nata de coco as precursor. The preparation process of PPy/BC nanocomposites is shown in Fig. 1. First, the BC hydrogel was broken by juicer processing and the obtained BC slurry diluted with deionized water to form a 400 mL solution with 0.25 wt% solid content. Next, 4 mL of concentrated HCl was added and stirred for 30 min. Second, 0.6 mL of Py was added into the above solution and continuously stirred for 3 h. Then, aqueous FeCl₃ (1 M) as oxidant was added to the pyrrole-containing solution, with the molar ratio of

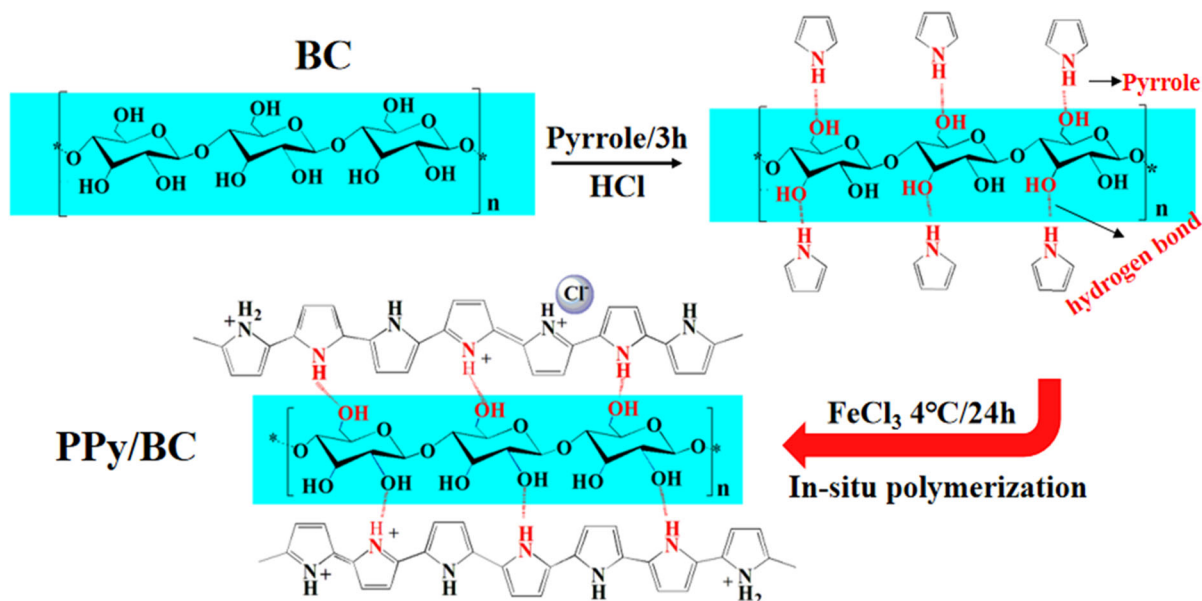


Fig. 1 Preparation process of PPy/BC nanocomposite

FeCl_3 /pyrrole molar ratio set at 2.4/1. All the above step were performed at room temperature. After that, the mixture was placed in a 4 °C refrigerator for 24 h and the resulting composites suction-filtered in air and washed with distilled water and ethanol until neutral filtrate. Finally the material was subjected to solvent exchange with *t*-butanol and freeze-dried at -50 °C and 20 Pa. In some procedures, the oxidant was replaced with ammonium persulfate or hydrogen peroxide, with the rest of the procedure the same. Unless otherwise specified, PPy/BC in this paper represents the material obtained using FeCl_3 as oxidant.

Characterization of adsorbents

The morphology and size of BC and PPy/BC were characterized using scanning electron microscopy (SEM; Nova NanoSEM 430, FEI Co., Hillsboro, OR, USA) and transmission electron microscopy (TEM; JEM-2100F, JEOL Ltd., Tokyo, Japan). Energy dispersive X-ray spectroscopy (EDX) elemental maps were obtained during SEM testing. The specific surface area of PPy/BC was measured through N_2 adsorption/desorption isotherms obtained at 77 K with an ASAP 2460 gas adsorption apparatus (Micromeritics Instrument Corp., Norcross, GA, USA). To analyze the functional groups of the samples,

infrared (IR) spectra were identified using an attenuated total reflectance-Fourier transform-infrared spectrometer (ATR-FT-IR; Nicolet iS50, Nicolet Instrument Corp., Madison, WI, USA) with a resolution of 4 cm^{-1} . Zeta (ζ)-potential measurements were performed using a zetasizer (Nano ZS90, Malvern Instruments Ltd., Worcestershire, UK). Surface chemical compositions of PPy/BC before and after water treatment were determined based on X-ray photoelectron spectroscopy (XPS; Axis Ultra DLD, Kratos Analytical Ltd., Manchester, UK).

Adsorption experiments

All adsorption experiments were conducted in plastic bottles, which were agitated in a thermostatic shaker at 200 rpm. Except for special instructions, adsorption experiments were executed by adding 15 mg of adsorbent to 60 mL of Cr(VI) aqueous solution. After the defined adsorption time, samples were retrieved using a $0.45\ \mu\text{m}$ membrane filter. Absorbance was measured using a UV-spectrophotometer at λ_{max} of 540 nm after the filtrate was reacted with 1,5-diphenylcarbazide to form a Cr(VI) complex, from which the Cr(VI) concentration was calculated from a standard curve.

The $100\ \text{mg L}^{-1}$ Cr(VI) solutions with initial pH from 2 to 8 were prepared to clarify the impact of

solution pH on Cr(VI) adsorption. In order to further study the practical application effect of PPy/BC and the competitive strength of adsorption sites in the presence of different ions, the effect of Cd^{2+} , Cu^{2+} , Zn^{2+} , SO_4^{2-} and NO_3^- with the same concentration on the adsorption of Cr(VI) by PPy/BC were studied. For adsorption kinetics, 75 mg composites were added to 300 mL of Cr(VI) solution (pH 2) with initial concentrations of 100, 150, and 200 mg L^{-1} . In addition, adsorption isotherm experiments were carried out at different temperatures (298, 308, and 318 K) and samples dispersed into Cr(VI) solutions (pH 2) of different initial concentrations (50, 100, 150, 200, 250, and 300 mg L^{-1}). According to the resulting equilibrium adsorption data, thermodynamic parameters, such as ΔG^0 , ΔH^0 , and ΔS^0 , were determined.

Five cycles of Cr(VI) adsorption and desorption were carried out to evaluate the reusability of PPy/BC nanofiber composites. In each cycle, 15 mg PPy/BC was added to 60 mL Cr(VI) solution (100 ppm and pH 2) and agitated for 24 h. Next, the Cr(VI)-loaded PPy/BC was stirred in 0.5 M NaOH solution for 1 h to accomplish desorption. Adsorption sites of the PPy/BC were regenerated by adding 1 M HCl solution and stirred for 1 h. After that, the adsorbent was washed with deionized water until neutral and then reused for the next adsorption test.

All adsorption experiments were performed in triplicate and expressed as averages, with all errors < 3%.

Results and discussion

Characterization

The surface morphology of BC and PPy/BC nanofiber composites were observed by SEM and TEM. BC was observed to have a nanoscale fiber structure, which provided a large number of adsorption sites for pyrrole monomers (Fig. 2a). After in situ oxidative polymerization, the PPy/BC diameters were significantly higher than that of BC (Fig. 2b). In addition, after the polymerization process, PPy maintained a perfect fiber structure without agglomeration. From TEM images, surface of PPy/BC was observed to be rough and PPy evenly wrapped on BC surfaces, forming a core-shell structure with a diameter of ~ 90 nm (Fig. 2c). According to the N_2 adsorption/desorption

curves, the BET specific surface area (S_{BET}) of PPy/BC was calculated to be 95.9 $\text{m}^2 \text{g}^{-1}$. The SEM and TEM images of PPy/BC prepared with ammonium persulfate and hydrogen peroxide as oxidants are shown in Fig. S1 and S2, respectively. The PPy/BC prepared by ammonium persulfate is partially agglomerated, and the adsorbent forms a beadlike structure (Fig. S1), and the caking was more severe when hydrogen peroxide was used as an oxidant (Fig. S2). Compared with the S_{BET} of PPy composites listed in Table 1, PPy/BC with higher specific surface area had better adsorption properties. In addition, the zeta potential of PPy/BC was measured. The point of zero charge (isoelectric point) was found to occur at $\text{pH} \sim 6$, below which the nitrogen atoms were protonated, which would have facilitated electrostatic attractions between anions and cations (Fig. 2d).

The chemical structures of the BC, PPy, and PPy/BC were characterized by FT-IR and it was observed that pure BC exhibited typical IR absorption peaks of cellulose, such as $-\text{OH}$ stretching (3345 cm^{-1}), $-\text{CH}_2-$ stretching (2895 cm^{-1}), and $\text{C}-\text{O}-\text{C}$ stretching (1057 cm^{-1}) (Fig. 2e; Cai et al. 2018). However, PPy/BC mainly showed characteristic peaks of PPy, with peaks at 1554 and 1456 cm^{-1} attributed to conjugated $\text{C}-\text{C}$ and $\text{C}-\text{N}$ stretching vibrations. Bands at 1305 and 1165 cm^{-1} are assigned to $\text{C}-\text{N}$ in-plane deformation and pyrrole ring breathing. Bands at 1034, 965, and 849 cm^{-1} derived from $\text{C}-\text{H}$ out-plane and in-plane bending and $\text{N}-\text{H}$ wagging of PPy in the PPy/BC, respectively (Wang et al. 2012; Yuan et al. 2019). In addition, it was noteworthy that the above peaks possessed a clear blue shift compared with pure PPy. This shift was due to $-\text{OH}$ groups of BC and $-\text{NH}$ groups in the pyrrole ring forming hydrogen bonds, which affected skeletal vibrations of the PPy chain (Xu et al. 2013).

Effects of initial pH

The solution pH is a crucial factor during the Cr(VI) adsorption process (Niu et al. 2017) and, here, the removal efficiency was found to reach 97.5% at pH 2 (Fig. 3). With increased pH, PPy/BC adsorption performance gradually deteriorated and the removal efficiency only 31.9% at pH 8. This change was related to the situation of Cr(VI) in different pH solutions. At pH 1, Cr(VI) in the solution mainly exists as H_2CrO_4 and cannot be adsorbed (Nezhad A A et al. 2018). At

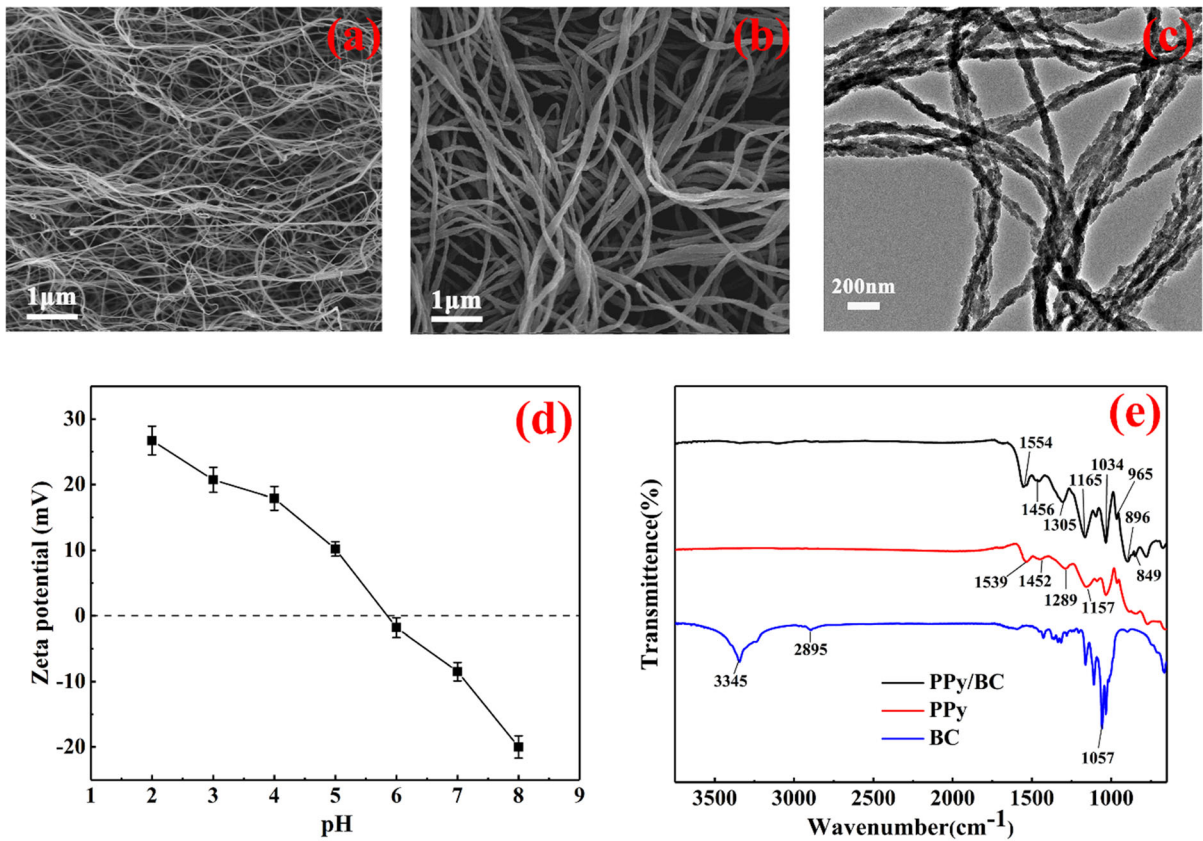


Fig. 2 SEM images of BC (a); PPy/BC (b); TEM image of PPy/BC (c); zeta-potential of PPy/BC with various pH in deionized water (d); and FTIR spectra of BC, PPy, and PPy/BC (e)

Table 1 Comparison of Cr(VI) adsorption performance of adsorbents at 298 K

Adsorbents	q_m (mg g ⁻¹)	Specific surface area (m ² g ⁻¹)	References
PPy/carbon black composites	174.81	64.47	(Ko et al.2018)
PPy/OMWCNTs	294.1	34.1	(Bhaumik et al.2016)
Bamboo-like PPy nanotubes	482.6	–	(Li et al.2012)
Graphene/Fe ₃ O ₄ @PPy nanocomposites	348.4	60.85	(Yao et al.2014)
PPy-Fe ₃ O ₄ /rGO composites	293.3	80.53	(Wang et al.2015)
Graphene/SiO ₂ @PPy nanocomposites	429.2	37.6	(Fang et al.2018)
Sulfuric acid modified leaves	107.53	–	(Zhang et al.2019)
Biochar modified with Mg/Al-layered double hydroxide intercalated with EDTA	38	–	(Huang et al.2019)
Polyaniline-coated electrospun adsorbent membrane	15.08	–	(Dognani et al.2019)
PPy/BC (APS)	372.8	72.1	This work
PPy/BC (FeCl ₃)	555.6	95.9	This work

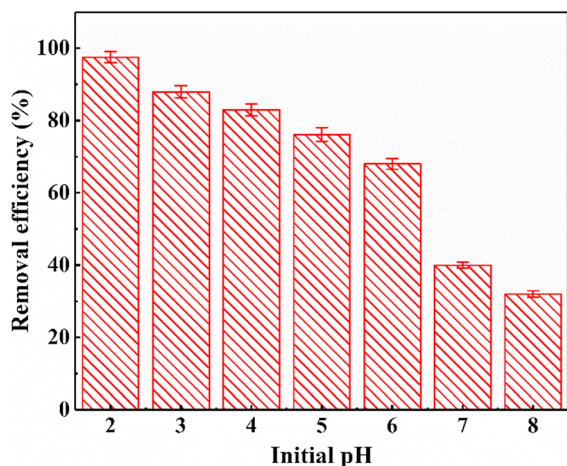
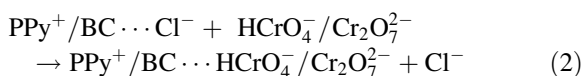
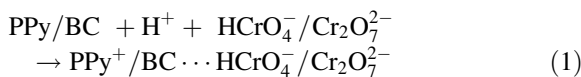


Fig. 3 Effects of pH on Cr(VI) removal efficiency by PPY/BC

pH 2–6, Cr(VI) mainly exists as HCrO_4^- and $\text{Cr}_2\text{O}_7^{2-}$. Once the pH is > 6 , the dominant species is CrO_4^{2-} (Dognani et al. 2019). From the Zeta potential results, we can know that the high adsorption efficiency at low pH condition is due to the strong electrostatic attraction among positively charged nitrogen (N^+) with chromium anion groups, as Eq. (1). In addition, Cl^- doped into PPY during polymerization can be ion exchanged with HCrO_4^- or $\text{Cr}_2\text{O}_7^{2-}$, as Eq. (2). When the pH value is greater than 6, the chromium anion will compete with OH^- for the adsorption position on the adsorbent surface, which makes the Cr(VI) adsorption capacity of PPY/BC decrease rapidly (Zhan et al. 2018).



The solution pH after adsorption equilibrium (pH_{eq}) was compared with that before adsorption (pH_i , Fig. S3). When the pH_i was < 6 , pH_{eq} was clearly larger than pH_i , which might be attributed to partial H^+ consumption during PPY protonation. However, when pH_i was > 6 , pH_{eq} and pH_i were similar.

Influence of interfering ions

It can be seen from the Fig. 4 that when the solution contained Cd^{2+} , Cu^{2+} , or Zn^{2+} , the effects of interfering ions on Cr(VI) removal from solution were

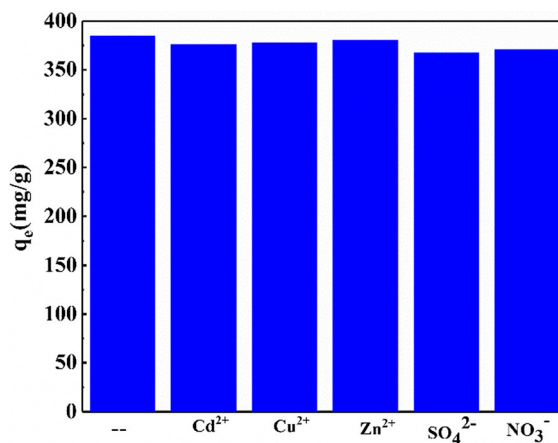


Fig. 4 Effects of coexisting ions on Cr(VI) adsorption on PPY/BC composite

small, which was mainly because that the surface protonation of in acidic environment makes PPY/BC produce electrostatic repulsion to cations. Thus, the effect of cations was negligible. When SO_4^{2-} and NO_3^- are present in the solution, their low affinity with the surface active sites of PPY makes them at a disadvantage in the competition with Cr(VI) (Chauke et al. 2015). Therefore, in general, the coexisting ions were observed to have little effect on the adsorption performance of PPY/BC.

Adsorption kinetics

The effects of reaction time on Cr(VI) adsorption capacity at different initial concentrations were investigated (Fig. 5a). The adsorption capacity of PPY/BC was seen to increase rapidly in the first 3 h and the growth rate gradually slowed down with time until adsorption equilibrium was reached. The pseudo-first-order and pseudo-second-order kinetic models were used to describe the kinetic adsorption process (Jung et al. 2018). The Cr(VI) adsorption kinetic data were fitted using linearized forms of the two kinetic models (Fig. S5); the corresponding parameters are listed in Table S1. By comparing the correlation coefficients (R^2), the pseudo-second-order kinetic model was observed to be more suitable for describing Cr(VI) adsorption kinetic data. The equilibrium adsorption capacity calculated according to this model [$q_e(\text{cal})$] was closer to the experimental values [$q_e(\text{exp})$], which indicated that PPY/BC adsorption Cr(VI) was controlled by the chemical reaction rate (Yao et al. 2014).

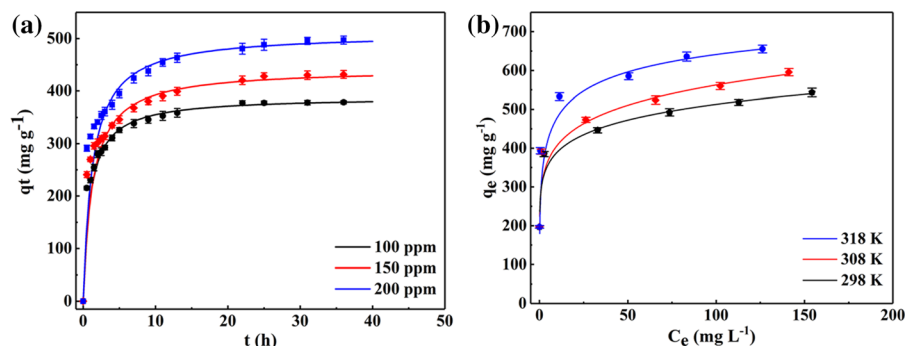


Fig. 5 Effects of contact time on Cr(VI) adsorption capacity with different initial concentrations and fit of kinetic date with nonlinear pseudo-second-order kinetic model **(a)** and

equilibrium isotherms of Cr(VI) adsorption onto PPy/BC and nonlinear plots of Langmuir model **(b)**

Adsorption isotherms

The equilibrium adsorption isotherm is an important means for studying the interaction behaviour between PPy/BC and Cr(VI). The equilibrium adsorption data at three temperatures (298, 308, and 318 K) was studied using the Langmuir and Freundlich adsorption isotherm models (Fig. 5b, Barrie et al. 2018). The linear plots and relevant parameters are shown in Figure S4 and Table S2. According to the correlation coefficients (R^2), the adsorption data was judged to be better described by the Langmuir model, which indicated that the adsorption process of PPy/BC was primarily a monolayer adsorption. In addition, the maximum adsorption capacity of PPy/BC increased from 555.6 (298 K) to 666.7 mg g^{-1} (318 K) with increased temperature. Compared with the adsorbents reported in the literature listed in Table 1, it was clear that PPy/BC had the better adsorption performance.

Adsorption thermodynamics

The thermodynamic parameters related to adsorption of Cr(VI) on PPy/BC, such as enthalpy change (ΔH^0 , $\text{kJ}\cdot\text{mol}^{-1}$), standard Gibbs free energy change (ΔG^0 , $\text{kJ}\cdot\text{mol}^{-1}$), and entropy change (ΔS^0 , $\text{J}\cdot\text{mol}^{-1}\cdot\text{K}^{-1}$) can be calculated by the following Eqs. (3–5) (Zhang et al. 2018):

$$\Delta G^0 = -RT \ln K_d \quad (3)$$

$$\ln K_d = \frac{\Delta S^0}{R} - \frac{\Delta H^0}{RT} \quad (4)$$

$$K_d = \frac{q_e}{C_e} \quad (5)$$

where R is the ideal gas constant ($8.314 \text{ J mol}^{-1} \cdot \text{K}^{-1}$), T (K) the absolute temperature, and K_d ($\text{L}\cdot\text{mol}^{-1}$) the thermodynamic equilibrium constant. Here, ΔH^0 and ΔS^0 were calculated from the slope and intercept of the plot of $\ln K_d$ versus $1/T$ (Fig. S6), with ΔG^0 , ΔH^0 , and ΔS^0 results shown in Table S3. The decrease in ΔG^0 values with increasing temperatures showed that higher temperature promoted Cr(VI) adsorption by PPy/BC due to a larger adsorption driving force. The positive value of ΔH^0 was in accord with the endothermic nature of the adsorption process. The positive value of ΔS^0 was due to Cl^- ion release on PPy/BC surfaces during the adsorption process, thereby increasing disorder of the PPy/BC-liquid interface (Bhaumik et al. 2012).

Recycle and desorption

The reusability and stability of an adsorbent are very important in practical applications. The results of PPy/BC regeneration and reusability testing showed that, after the fifth recycle, the adsorbent retained 70.5% of its initial adsorption capacity, showing that PPy/BC possessed great regeneration stability (Fig. 6a). Comparing SEM images of PPy/BC before adsorption and after the fifth recycle showed that there was no significant difference, which indicated that PPy was firmly wrapped on BC surfaces during the adsorption process and prevented secondary pollution (Figs. 2b and 6b). This indicates that the recoverability of the occupied adsorption sites is effective and the PPy/BC is stable in the adsorption process.

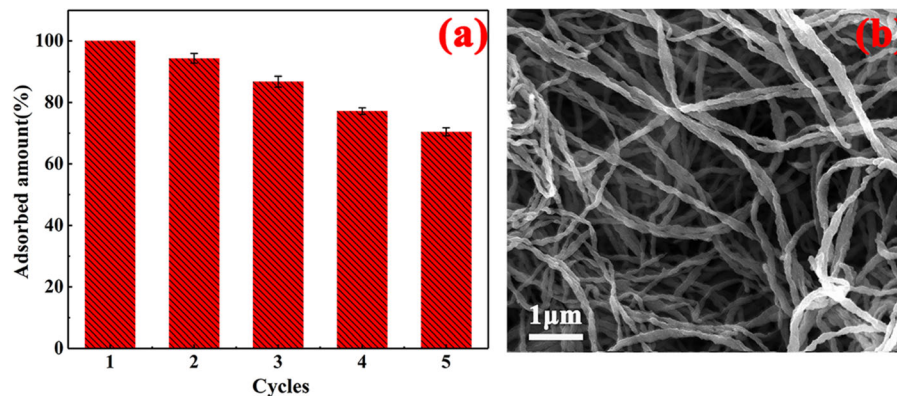


Fig. 6 Adsorption/desorption cycles of PPy/BC in Cr(VI) adsorption (a) and SEM image of PPy/BC after fifth recycle (b)

Adsorption mechanism of Cr(VI) by PPy/BC

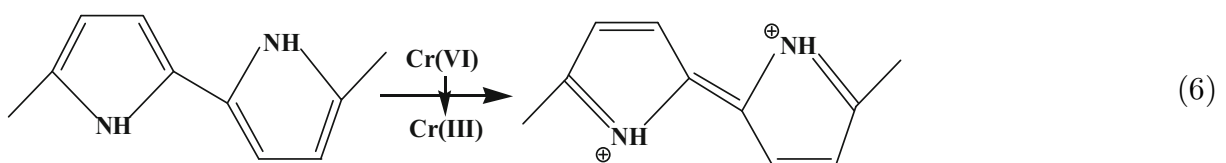
Figure S7a shows the digital photographs for removal of Cr(VI) by PPy/BC. After adsorption, the PPy/BC was determined by SEM–EDX. Two strong peaks at 0.6 keV and 5.4 keV in EDX spectrum (Fig. S7b) correspond to Cr(VI). Meanwhile, the content can reach 27.2 wt% through quantitatively analyzed of X-ray elemental mapping, which indicates that the PPy/BC could effectively remove Cr(VI).

FT-IR spectra of PPy/BC after Cr(VI) adsorption showed that most peaks shifted to higher wavenumbers, compared to those of PPy/BC before adsorption (Figs. 7a and 2e, respectively). The peaks at 1456 cm^{-1} (C–N stretching vibrations) and 849 cm^{-1} (N–H bending vibrations) disappeared, and the pyrrole ring breathing band shifted significantly (from 1165 to 1207 cm^{-1}). These results could have been due to the existence of Cr(VI) on PPy/BC, which agitated the PPy conjugate structure and limited the extent of polymer chain charge delocalization (Setshedi et al. 2013).

XPS was used to characterize the change in chemical composition of PPy/BC surface before and after adsorption (Fig. 7b). It can be seen that three strong peaks at binding energies of 532.2, 399.8 and

284.8 eV which corresponding to O 1 s, N 1 s and C 1 s, respectively (Wan et al. 2017). After adsorption of Cr(VI), the peak corresponding to Cr 2p appears. The high resolution of Cr 2p spectrum can be split into two peaks at 586.7 eV and 576.9 eV, corresponding to Cr $2p_{1/2}$ and Cr $2p_{3/2}$ (Ballav et al. 2012; Zhang et al. 2016). In addition, the O1s peak is significantly enhanced, and the C/O ratio is significantly lower than before adsorption. This may be due to the adsorption of chromium anion groups containing oxygen atoms. The adsorption mechanism was further explored by examining high-resolution Cr-2p spectra, after deconvolution of the Cr-2p peak, both Cr(VI) and Cr(III) existed on PPy/BC surfaces with their molar ratios at 40.4 and 59.6%, respectively (Fig. 7c). This indicates that part of Cr(VI) is reduced to Cr(III) by electron-rich PPy (Zhao J et al. 2015; Fang W et al. 2018).

Furthermore, the N-1 s spectra of PPy/BC before and after adsorption was divided into three peaks, as =N–, –NH–, and N^+ (Fig. 7d). After Cr(VI) adsorption, the molar ratio of –NH– units decreased from 57.6 to 45.1%, while the molar ratio of =N– units increased from 14.1 to 30.7%. This may be due to the strong oxidation of Cr(VI) (Wang et al. 2015). The following reactions might have occurred:



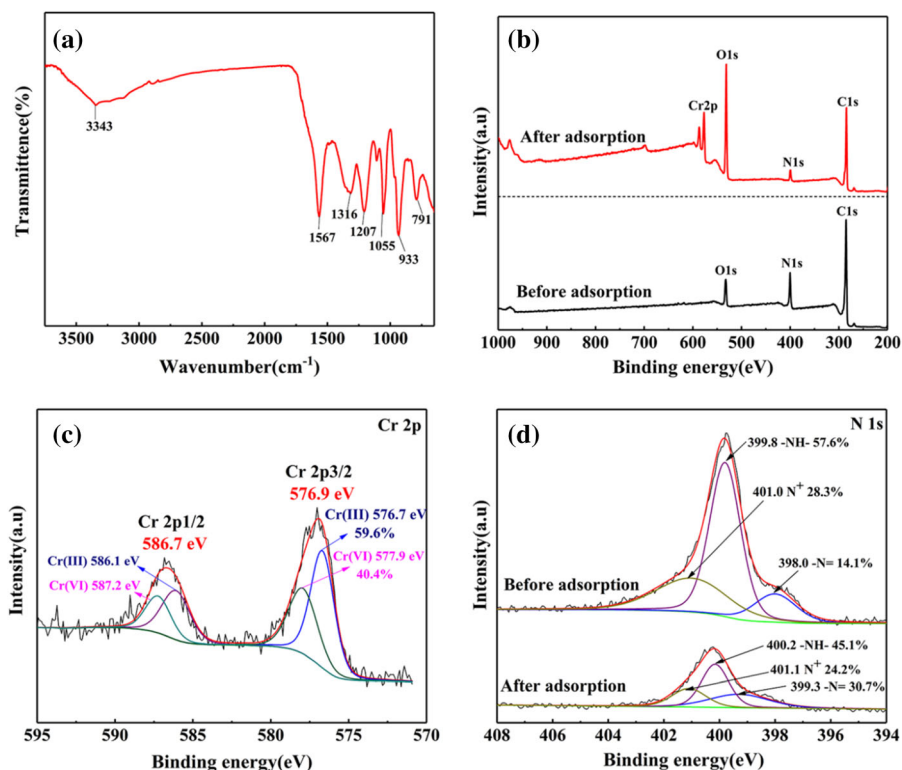


Fig. 7 FTIR spectrum of PPy/BC after adsorption of Cr(VI) (a), and XPS spectra of PPy/BC with survey scan (b), Cr-2p high-resolution spectra (c), and N-1 s high-resolution spectra (d)

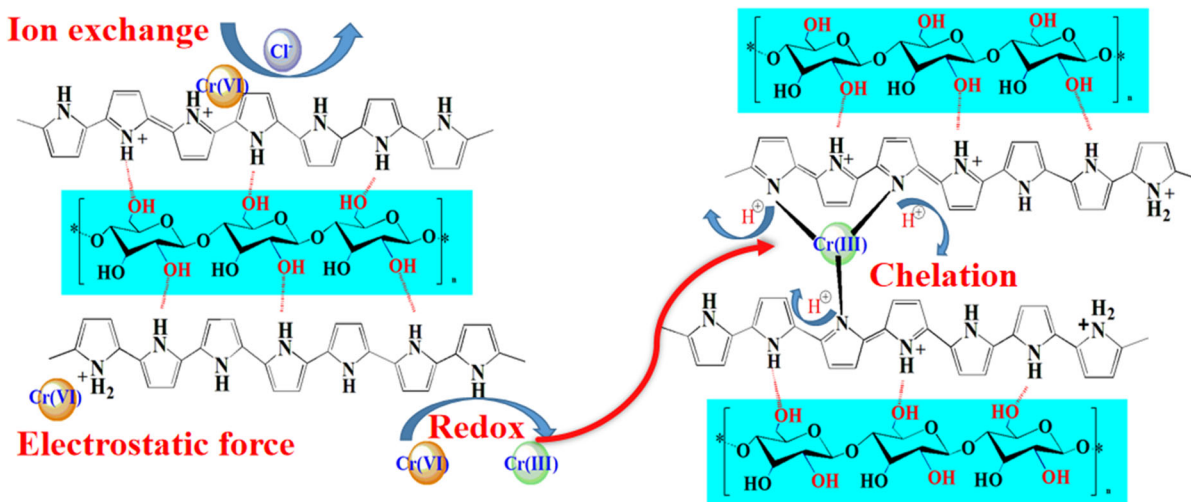


Fig. 8 The mechanism of PPy/BC nanocomposite to remove Cr (VI)

This was similar to the behavior of many reported adsorbents (Zhao et al. 2015; Guo et al. 2018). According to the theory of hard and soft acids and bases, amine groups are hard base, which has a strong

chelation with hard acid Cr(III) (Deng et al. 2004). Cr(III) can be adsorbed on the deprotonated pyrrole amine groups by chelation.

In general, the removal mechanism of Cr(VI) by PPy/BC is shown in Fig. 8, which mainly including: (1) the Cr(VI) anion group and the proton nitrogen (N^+) generate electrostatic attraction and are adsorbed to the surface of PPy/BC; (2) the ion exchange occurs between Cr(VI) and PPy doped Cl^- during polymerization; (3) Cr(VI) was partially reduced to Cr(III) - while the -NH- functional group in the ppyrrole was converted to = N-, and the Cr (III) was immobilized on the surface of adsorbent by chelation with the deprotic PPy amino group.

Conclusions

In this study, a cost-effective and high-performance adsorbent of PPy/BC nanofiber composites for wastewater Cr(VI) removal was successfully prepared by simple in situ oxidative polymerization. Using the Langmuir isotherm model, the calculated adsorption capacity of PPy/BC reached 555.6 mg g^{-1} at 298 K. The adsorption capacity was strongly dependent on pH and the optimal pH 2. The removal process of Cr(VI) by PPy/BC included ion exchange between Cl^- and Cr(VI), electrostatic attraction between Cr(VI) and protonated PPy, and a reduction process from high-toxicity Cr(VI) to low-toxicity Cr(III). Moreover, compared with many artificial nanoparticle adsorbents, PPy/BC showed great advantages in operability of preparation and separation processes. Although the diameter of BC is about 90 nm, its length reaches the micron scale, so compared with other artificial nanoparticles, it has better separation performance. In fact, we can better achieve water and adsorbent separation through the negative pressure screen, using filter paper. And the adsorption capacity of PPy/BC is several times that of other sheet or block PPy composites. In addition, recycling results demonstrated that PPy/BC well retained its abilities. In general, this study provided a solution for the effective treatment of Cr(VI) polluted water using a green adsorbent.

Acknowledgments The authors appreciate the financial support of Guangdong Water Conservancy Science and Technology Innovation Project (No. 2020-10).

Compliance with ethical standards

Conflict of interest The authors declare that they have no conflict of interest.

References

- Ballav N, Maity A, Mishra SB (2012) High efficient removal of chromium(VI) using glycine doped polypyrrole adsorbent from aqueous solution. *Chem Eng J* 198–199:536–546
- Barnie S, Zhang J, Wang H, Yin H, Chen H (2018) The influence of pH, co-existing ions, ionic strength, and temperature on the adsorption and reduction of hexavalent chromium by undissolved humic acid. *Chemosphere* 212:209–218. <https://doi.org/10.1016/j.chemosphere.2018.08.067>
- Bhaumik M, Maity A, Srinivasu VV, Onyango MS (2012) Removal of hexavalent chromium from aqueous solution using polypyrrole-polyaniline nanofibers. *Chem Eng J* 181:323–333. <https://doi.org/10.1016/j.cej.2011.11.088>
- Bhaumik M, Agarwal S, Gupta VK, Maity A (2016) Enhanced removal of Cr(VI) from aqueous solutions using polypyrrole wrapped oxidized MWCNTs nanocomposites adsorbent. *J Colloid Interface Sci* 470:257–267. <https://doi.org/10.1016/j.jcis.2016.02.054>
- Cai M, Shafi S, Zhao Y (2018) Preparation of compressible silica aerogel reinforced by bacterial cellulose using tetraethylorthosilicate and methyltrimethoxysilane coprecursor. *J Non-Cryst Solids* 481:622–626. <https://doi.org/10.1016/j.jnoncrysol.2017.12.015>
- Chauke VP, Maity A, Chetty A (2015) High-performance towards removal of toxic hexavalent chromium from aqueous solution using graphene oxide-alpha cyclodextrin-polypyrrole nanocomposites. *J Mol Liq* 211:71–77
- Demiral H, Demiral I, Tumsek F, Karabacakoglu B (2008) Adsorption of chromium (VI) from aqueous solution by activated carbon derived from olive bagasse and applicability of different adsorption models. *Chem Eng J* 144:188–196
- Deng S, Bai R (2004) Removal of trivalent and hexavalent chromium with aminated polyacrylonitrile fibers: performance and mechanisms. *Water Res* 38:2423–2431
- Dognani G, Hadi P, Ma H, Cabrera FC, Job AE, Agostini DL, Hsiao BS (2019) Effective chromium removal from water by polyaniline-coated electrospun adsorbent membrane. *Chem Eng J* 372:341–351. <https://doi.org/10.1016/j.cej.2019.04.154>
- Fang W, Jiang X, Luo H, Geng J (2018) Synthesis of graphene/SiO₂@ polypyrrole nanocomposites and their application for Cr(VI) removal in aqueous solution. *Chemosphere* 197:594–602. <https://doi.org/10.1016/j.chemosphere.2017.12.163>
- Gheju M, Balcu I (2011) Removal of chromium from Cr(VI) polluted wastewaters by reduction with scrap iron and subsequent precipitation of resulted cations. *J Hazard Mater* 196:131–138. <https://doi.org/10.1016/j.jhazmat.2011.09.002>

- Guan X, Yang H, Sun Y, Qiao J (2019) Enhanced immobilization of chromium(VI) in soil using sulfidated zero-valent iron. *Chemosphere* 228:370–376. <https://doi.org/10.1016/j.chemosphere.2019.04.132>
- Guo DM, An QD, Xiao ZY, Zhai SR, Yang DJ (2018) Efficient removal of Pb(II), Cr(VI) and organic dyes by polydopamine modified chitosan aerogels. *Carbohydr Polym* 202:306–314. <https://doi.org/10.1016/j.carbpol.2018.08.140>
- Huang D, Liu C, Zhang C, Deng R, Wang R, Xue W, Luo H, Zeng G, Zhang Q, Guo X (2019) Cr(VI) removal from aqueous solution using biochar modified with Mg/Al-layered double hydroxide intercalated with ethylenediaminetetraacetic acid. *Bioresour Technol* 276:127–132. <https://doi.org/10.1016/j.biortech.2018.12.114>
- Jin W, Du H, Zheng S, Zhang Y (2016) Electrochemical processes for the environmental remediation of toxic Cr(VI): a review. *Electrochim Acta* 191:1044–1055. <https://doi.org/10.1016/j.electacta.2016.01.130>
- Jin X, Xiang Z, Liu Q, Chen Y, Lu F (2017) Polyethyleneimine-bacterial cellulose bioadsorbent for effective removal of copper and lead ions from aqueous solution. *Bioresour Technol* 244:844–849. <https://doi.org/10.1016/j.biortech.2017.08.072>
- Jung KW, Lee SY, Lee YJ (2018) Facile one-pot hydrothermal synthesis of cubic spinel-type manganese ferrite/biochar composites for environmental remediation of heavy metals from aqueous solutions. *Bioresour Technol* 261:1–9. <https://doi.org/10.1016/j.biortech.2018.04.003>
- Ko YJ, Choi K, Lee S, Jung KW, Hong S, Mizuseki H, Choi JW, Lee WS (2018) Strong chromate-adsorbent based on pyrolic nitrogen structure: an experimental and theoretical study on the adsorption mechanism. *Water Res* 145:287–296. <https://doi.org/10.1016/j.watres.2018.08.033>
- Li S, Lu X, Li X, Xue Y, Zhang C, Lei J, Wang C (2012) Preparation of bamboo-like PPy nanotubes and their application for removal of Cr(VI) ions in aqueous solution. *J Colloid Interface Sci* 378:30–35. <https://doi.org/10.1016/j.jcis.2012.03.065>
- Mahmud HNME, Huq AO, Yahya R (2016) The removal of heavy metal ions from wastewater/aqueous solution using polypyrrole-based adsorbents: a review. *RSC Adv* 6:14778–14791. <https://doi.org/10.1039/C5RA24358K>
- Molaei K, Bagheri H, Asgharinezhad AA, Ebrahimzadeh H, Shamsipur M (2017) SiO₂-coated magnetic graphene oxide modified with polypyrrole–polythiophene: a novel and efficient nanocomposite for solid phase extraction of trace amounts of heavy metals. *Talanta* 167:607–616. <https://doi.org/10.1016/j.talanta.2017.02.066>
- Nezhad AA, Alimoradi M, Ramezani M (2018) One-step preparation of graphene oxide/polypyrrole magnetic nanocomposite and its application in the removal of methylene blue dye from aqueous solution. *Mater Res Express* 5(2):025508
- Niu Y, Li K, Ying D, Wang Y, Jia J (2017) Novel recyclable adsorbent for the removal of copper(II) and lead(II) from aqueous solution. *Bioresour Technol* 229:63–68. <https://doi.org/10.1016/j.biortech.2017.01.007>
- Roy K, Mondal P, Bayen SP, Chowdhury P (2012) Sonochemical synthesis of polypyrrole salt and study of its Cr(VI) sorption-desorption properties. *J Macromol Sci A* 49:931–935. <https://doi.org/10.1080/10601325.2012.722852>
- Sai H, Fu R, Xing L, Xiang J, Li Z, Li F, Zhang T (2015) Surface modification of bacterial cellulose aerogels' web-like skeleton for oil/water separation. *ACS Appl Mater Inter* 7:7373–7381. <https://doi.org/10.1021/acsami.5b00846>
- Setshedi KZ, Bhaumik M, Songwane S, Onyango MS, Maity A (2013) Exfoliated polypyrrole-organically modified montmorillonite clay nanocomposite as a potential adsorbent for Cr(VI) removal. *Chem Eng J* 222:186–197. <https://doi.org/10.1016/j.cej.2013.02.061>
- Wan C, Jiao Y, Li J (2017) Flexible, highly conductive, and free-standing reduced graphene oxide/polypyrrole/cellulose hybrid papers for supercapacitor electrodes. *J Mater Chem A* 5:3819–3831. <https://doi.org/10.1039/C6TA04844G>
- Wang H, Yuan X, Wu Y, Chen X, Leng L, Wang H, Li H, Zeng G (2015) Facile synthesis of polypyrrole decorated reduced graphene oxide–Fe₃O₄ magnetic composites and its application for the Cr(VI) removal. *Chem Eng J* 262:597–606. <https://doi.org/10.1016/j.cej.2014.10.020>
- Wang J, Tavakoli J, Tang Y (2019) Bacterial cellulose production, properties and applications with different culture methods—a review. *Carbohydr Polym* 219:63–76. <https://doi.org/10.1016/j.carbpol.2019.05.008>
- Wang Y, Zou B, Gao T, Wu X, Lou S, Zhou S (2012) Synthesis of orange-like Fe₃O₄/PPy composite microspheres and their excellent Cr(VI) ion removal properties. *J Mater Chem* 22:9034–9040. <https://doi.org/10.1039/C2JM30440F>
- Wu ZY, Liang HW, Chen LF, Hu BC, Yu SH (2015) Bacterial cellulose: a robust platform for design of three dimensional carbon-based functional nanomaterials. *Acc Chem Res* 49:96–105. <https://doi.org/10.1021/acs.accounts.5b00380>
- Xu J, Zhu L, Bai Z, Liang G, Liu L, Fang D, Xu W (2013) Conductive polypyrrole–bacterial cellulose nanocomposite membranes as flexible supercapacitor electrode. *Org Electron* 14:3331–3338. <https://doi.org/10.1016/j.orgel.2013.09.042>
- Xu Y, Wang D, Xie M, Jing L, Huang Y, Huang L, Xu H, Li H, Xie J (2019) Novel broad spectrum light responsive PPy/hexagonal-SnS₂ photocatalyst for efficient photoreduction of Cr(VI). *Mater Res Bull* 112:226–235. <https://doi.org/10.1016/j.materresbull.2018.12.017>
- Yao W, Ni T, Chen S, Li H, Lu Y (2014) Graphene/Fe₃O₄@-polypyrrole nanocomposites as a synergistic adsorbent for Cr(VI) ion removal. *Compos Sci Technol* 99:15–22. <https://doi.org/10.1016/j.compscitech.2014.05.007>
- Yuan X, Floresyona D, Aubert PH, Bui TT, Remita S, Ghosh S, Brisset F, Goubard F, Remita H (2019) Photocatalytic degradation of organic pollutant with polypyrrole nanostructures under UV and visible light. *Appl Catal B-Environ* 242:284–292. <https://doi.org/10.1016/j.apcatb.2018.10.002>
- Zhan Y, He S, Wan X, Zhang J, Liu B, Wang J, Li Z (2018) Easy-handling bamboo-like polypyrrole nanofibrous mats with high adsorption capacity for hexavalent chromium removal. *J Colloid Interface Sci* 529:385–395. <https://doi.org/10.1016/j.jcis.2018.06.033>

- Zhang L, Fang M (2010) Nanomaterials in pollution trace detection and environmental improvement. *Nano Today* 5:128–142. <https://doi.org/10.1016/j.nantod.2010.03.002>
- Zhang J, Chen H, Chen Z, He J, Shi W, Liu D, Chi H, Cui F, Wang W (2016) Microstructured macroporous adsorbent composed of polypyrrole modified natural corncob-core sponge for Cr(VI) removal. *RSC Adv* 6:59292–59298. <https://doi.org/10.1039/C6RA07687D>
- Zhang Y, Li M, Li J, Yang Y, Liu X (2019) Surface modified leaves with high efficiency for the removal of aqueous Cr(VI). *Appl Surf Sci* 484:189–196. <https://doi.org/10.1016/j.apsusc.2019.04.088>
- Zhang Y, Lin S, Qiao J, Kołodyńska D, Ju Y, Zhang M, Cai M, Deng D, Dionysiou DD (2018) Malic acid-enhanced chitosan hydrogel beads (mCHBs) for the removal of Cr(VI) and Cu(II) from aqueous solution. *Chem Eng J* 353:225–236. <https://doi.org/10.1016/j.cej.2018.06.143>
- Zhao J, Li Z, Wang J, Li Q, Wang X (2015) Capsular polypyrrole hollow nanofibers: an efficient recyclable adsorbent for hexavalent chromium removal. *J Mater Chem A* 3:15124–15132. <https://doi.org/10.1039/C5TA02525G>

Publisher's Note Springer Nature remains neutral with regard to jurisdictional claims in published maps and institutional affiliations.